Eur J Nucl Med Mol Imaging (2014) 41:1408–1418
DOI 10.1007/s00259-014-2728-4

ORIGINAL ARTICLE

Insight on AV-45 binding in white and grey matter from histogram analysis: a study on early Alzheimer's disease patients and healthy subjects

Federico Nemmi · Laure Saint-Aubert · Djilali Adel · Anne-Sophie Salabert · Jérémie Pariente · Emmanuel J. Barbeau · Pierre Payoux · Patrice Péran

Received: 14 November 2013 / Accepted: 7 February 2014 / Published online: 27 February 2014

Abstract
Purpose AV-45 amyloid biomarker is known to show uptake in white matter in patients with Alzheimer's disease (AD), but also in the healthy population. This binding, thought to be of a non-specific lipophilic nature, has not yet been investigated. The aim of this study was to determine the differential pattern of AV-45 binding in white matter in healthy and pathological populations.
Methods We recruited 24 patients presenting with AD at an early stage and 17 matched, healthy subjects. We used an optimized positron emission tomography-magnetic resonance imaging (PET-MRI) registration method and an approach based on an intensity histogram using several indices. We compared the results of the intensity histogram analyses with a more canonical approach based on target-to-cerebellum Standard Uptake Value (SUVr) in white and grey matter using MANOVA and discriminant analyses. A cluster analysis on white and grey matter histograms was also performed.
Results White matter histogram analysis revealed significant differences between AD and healthy subjects, which were not revealed by SUVr analysis. However, white matter histograms were not decisive to discriminate groups, and indices based on grey matter only showed better discriminative power than SUVr. The cluster analysis divided our sample into two clusters, showing different uptakes in grey, but also in white matter.
Conclusion These results demonstrate that AV-45 binding in white matter conveys subtle information not detectable using the SUVr approach. Although it is not more efficient than standard SUVr in discriminating AD patients from healthy subjects, this information could reveal white matter modifications.

Keywords AV-45 · Amyloid · Intensity histogram · Discrimination analysis · Alzheimer's disease

Federico Nemmi and Laure Saint-Aubert contributed equally to this work.

Electronic supplementary material The online version of this article (doi:10.1007/s00259-014-2728-4) contains supplementary material, which is available to authorized users.

F. Nemmi (✉) · L. Saint-Aubert · D. Adel · A.-S. Salabert · J. Pariente · P. Payoux · P. Péran
Inserm, imagerie cérébrale et handicaps neurologiques UMR 825, Centre Hospitalier Universitaire de Toulouse, Place du Dr. Baylac, CHU Purpan, Pavillon Baudot, 31059 Toulouse cedex 9, France
e-mail: federico.nemmi@gmail.com

F. Nemmi · L. Saint-Aubert · D. Adel · A.-S. Salabert · J. Pariente · P. Payoux · P. Péran
Université de Toulouse, UPS, imagerie cérébrale et handicaps neurologiques UMR 825, Centre Hospitalier Universitaire de Toulouse, Toulouse, France

D. Adel · A.-S. Salabert · P. Payoux
Service de Médecine Nucléaire, Pôle Imagerie, Centre Hospitalier Universitaire de Toulouse, Toulouse, France

J. Pariente · E. J. Barbeau
Service de neurologie, pôle neurosciences, Centre Hospitalier Universitaire de Toulouse, Toulouse, France

E. J. Barbeau
Université de Toulouse, UPS, centre de recherche cerveau et cognition, CNRS, CerCo, Toulouse, France

Introduction

Florbetapir (AV-45) radioligand has been shown to bind to amyloid peptide with good affinity [1, 2]. Correlations between AV-45 uptake and in vivo location of amyloid plaques have also been shown [3, 4]. In positron emission tomography (PET) studies in vivo, Alzheimer's disease (AD) patients have been shown to have higher AV-45 retention than healthy

controls (HC) [5, 6], even at early stages of the disease [7]. These characteristics point to AV-45 uptake, together with other amyloid ligands, as a good biomarker of amyloid pathology and Alzheimer's disease, and as a possible aid to clinical diagnosis. In clinical practice, visual analysis is the most widely used method for exploiting AV-45 images, but although it is undoubtedly useful, such analysis can lead to limited sensitivity and specificity [8].

Most studies have thus far focused on voxel-wise analyses [9] and global AV-45 uptake [6]. However, AV-45 has also shown non-specific binding in white matter [6]. White matter is a tissue mainly composed of myelin, which is highly lipidic. The lipophilic nature of AV-45 [1, 9] may thus explain the non-specific binding in this tissue [8]. Consequently, both healthy subjects and AD patients show marked binding of AV-45 in white matter [6]. Furthermore, the lack of specific binding should lead to comparable uptake of AV-45 in the white matter of healthy subjects and AD patients. In attempts to avoid this issue, recent studies have used different methods in order to focus on AV-45 uptake in the grey matter, excluding white matter from the analysis [7, 10, 11]. Only a few previous studies have investigated differential binding of amyloid biomarkers in white matter tissue. The authors failed to find any difference in uptake by white matter between AD and HC, either using the fluoride amyloid marker florbetaben or the carbonate amyloid marker PiB [12–14]. To our knowledge, no study regarding the differential binding of AV-45 amyloid marker to white matter in AD patients and healthy controls has been conducted so far. Moreover, little is known about the differential AV-45 uptake observed between grey and white matter for each group.

The aim of this study was (1) to determine and compare the pattern of AV-45 binding in white matter in AD and HC, (2) to compare the binding patterns in white and grey matter within each group, and (3) to investigate whether more subtle uptake quantification can lead to better discrimination performance. For this purpose, we investigated AV-45 uptake in patients presenting with early-stage AD and matched, healthy subjects. In order to characterize AV-45 uptake in white and grey matter, we used an approach based on counts-per-second histograms.

Materials and methods

Subjects

All participants gave their written informed consent. This study was approved by the local ethics committee (Comité de Protection des Personnes Sud-Ouest et Outre-Mer I) and the French Agency for the Safety and Security of Medical Devices (Agence Française de Sécurité Sanitaire des Produits de Santé, reference A90605-58).

Patients over 65 years of age at the prodromal stage of Alzheimer's disease (AD) and matched healthy controls (HC) were recruited. All patients came from the outpatient memory clinic (Neurology department, University Hospital, Toulouse, France), and presented with a memory complaint dating from more than 6 months. They were selected according to research criteria for prodromal Alzheimer's disease [15]; i.e., they had to show isolated memory impairment on neuropsychological assessment and one or more of the following features:

- medial temporal lobe atrophy assessed on magnetic resonance imaging (MRI) scan (sequences detailed below);
- temporo-parietal hypometabolism pattern on cerebral fluorodeoxyglucose (FDG)-PET scan;
- abnormal cerebrospinal fluid (CSF) biomarkers according to published criteria [16]

Patients were not included if they had a history of concomitant neurological or psychiatric disease, or if they had any clinically significant pathology that could explain the memory complaint. Significant white matter hyperintensities found on T2 MRI scan were a motive for exclusion.

Healthy controls were recruited among patients' relatives, or using recruitment posting in public places. They were not included if they had any neurological or psychiatric disease history, or if they had first-degree relatives with Alzheimer's disease. They underwent the same neuropsychological assessment and the same imaging examinations (MRI, FDG-PET) as patients. They had no memory complaint, and showed neither cognitive impairment on the neuropsychological assessment nor abnormalities on MRI scan.

All participants included underwent a second PET-scan using florbetapir (AV-45) amyloid marker (details on acquisition below).

These examinations were spread over three different appointments, scheduled within 3 months maximum. More details on population recruitment are available elsewhere [7].

Image acquisition

A brain MRI scan was performed in all participants using a Philips 3-T imager (Intera Achieva, Philips, Best, The Netherlands). A high resolution anatomical image, using a 3D-T1 weighted sequence (in-plane resolution 1×1 mm, slice thickness 1 mm, repetition time/echo time/inversion time= 8189 ms/3.75 ms/1012.2 ms, flip angle 8°, field of view 240×256, and 160 contiguous slices) and a T2-weighted sequence (reconstructed resolution 0.45×0.45×3 mm^3, repetition time/echo time=4 132 ms/80 ms, flip angle 90°, field of view 240×184, and 43 slices) were achieved.

AV-45 combined PET-CT scans were performed on a hybrid PET/CT Biograph 6 TruePoint HiRez (Siemens medical Solutions). This PET/CT operated in three-dimensional (3D)

detection mode. The images were reconstructed using the 3D ordered subset expectation maximization (OSEM) algorithm (four iterations, 16 subsets), with corrections for random, scatter, and attenuation provided by the manufacturer. Partial volume effect correction was performed using the Point Spread Function (PSF) model implemented by Siemens (HD-PET©). The acquisitions were performed 50 min after intravenous administration of 3.4±0.4 MBq/kg of ^{18}F Florbetapir for 20 min of list-mode acquisitions.

Visual analysis

AV-45 PET scan images were visually assessed by three observers (two Nuclear Medicine physicians and one Radiology physicist) who followed a special training programme, blind to clinical diagnosis. Images were classified as amyloid-positive or negative by comparing the cortical grey and white matter AV-45 uptakes. Following the recommendations given by the AV-45 supplier (Lily®), a scan was rated as positive when contrast between grey and white matter was lost in two or more brain areas (each area being larger than a single cortical gyrus), or when the scan showed one or more areas (each area being larger than a single cortical gyrus) in which grey matter radioactivity was intense and clearly exceeded the radioactivity of adjacent white matter (http://pi.lilly.com/us/amyvid-uspi.pdf). Finally, the amyloid profile was considered positive when at least two observers rated the scan as positive; otherwise, it was considered negative. The discriminating power of AV-45 imaging visual rating was calculated using specificity (percentage of healthy controls rated amyloid negative) and sensitivity (percentage of AD patients rated amyloid positive). Fleiss' kappa was calculated as a measure of agreement [17].

Image analysis

Segmentation of grey and white matter was achieved using SIENAX and FIRST (FSL library tools) from the 3D-T1 MRI image of each participant. AV-45 images were registered onto the subjects' anatomical space defined by the T1 images. To do this, CT scans of each subject were first linearly registered to the relative T1 image. The transformation matrix obtained from this linear registration was then applied to the AV-45 images, so that AV-45 images were coregistered in the T1 space. For subsequent analysis, only data pertaining to grey and white matter were used (Fig. 1).

Standard uptake value calculation

In order to assess mean uptake, the mean count per voxel was extracted for all segmented AV-45 images for the grey and white matter separately. The maps of all the grey matter and all the white matter were taken into account for this quantification. These values were then divided by the mean count per voxel of the whole cerebellum (vermis excluded), in order to obtain the standard uptake value ratio [3, 6].

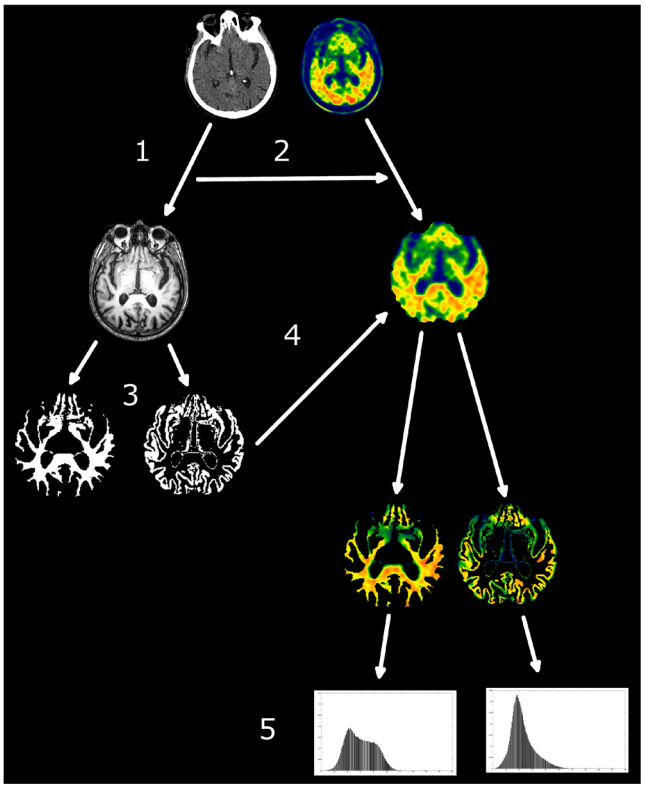

Fig. 1 Pipeline for histogram creation. CT scan was registered on the T1 scan (1) and the transformation matrix applied to the PET AV-45 scan (2). T1 was segmented into grey and white matter (3) and the binary masks of the tissues were applied to the PET AV-45 scan in T1 space (4). Intensity histograms were extracted from the tissues (5)

Mean SUVrs between AD and HC groups for white matter were compared using two-sample t-tests. This comparison was also made for grey matter. SUVr for grey and white matter were compared within each group using a Wilcoxon test.

Histograms

Histogram definition

Using FSL software, we created an AV-45-intensity (counts per second) histogram for grey and white matter for each subject. The intensity range of each image was divided into 200 bins and the frequency of occurrence of each intensity value (i.e., the number of voxels falling in that intensity range) was computed for each bin (see Fig. 1). In order to allow direct comparison between histograms, we divided the frequency of occurrence of each intensity bin by the total number of voxels in the tissue analysed.

To assess the possible effect the threshold chosen for the grey and white matter masks might have on the intensity histograms, we randomly chose one HC and one AD patient, and created grey and white matter masks using a probability

gradient: thresholds at 0.25, 0.50, 0.75 and 0.95., corresponding to probabilities of 25 %, 50 %, 75 % and 95 %, respectively, of the matter being grey/white. A histogram was then created for each of the masks (i.e., eight histograms per subject, four for grey matter and four for white matter) and the histograms were visually inspected for differences related to the chosen thresholds (supplementary Figure 1).

Finally, to rule out the possible effect of AV-45 signal spill out from grey to white matter, we calculated a conservative white matter mask. AV-45 white matter images were eroded using an isotropic Gaussian kernel of 1 mm in order to exclude white matter voxels bordering the grey matter voxels. The histograms were derived from these eroded images.

In a further effort to control for possible confounds in the white matter, we automatically segmented white matter hyperintensities for both AD and HC subjects and masked the white matter AV-45 images for these hyperintensities (see supplementary data for methodological details).

Histogram analysis

Different indices were extracted from the histograms of each subject in the grey and white matter separately. We calculated the 10th and 90th percentiles of occurrence frequency, the median bin, the kurtosis, the skewness, the maximal bin, the area under the curve below the maximal bin (ABM), the maximum frequency and the histogram width. These indices are among the most commonly used in histogram analyses [18–20].

To assess the relationship between white and grey matter within each subject, we calculated the Euclidean distance between the peaks of white and grey matter histograms. The difference between Euclidean distances in the two groups was assessed by a two-sample *t*-test.

Given the non-Gaussian distribution of the different indices, data were first transformed into ranks in order to carry out a parametric statistical test [21]. The ranked histogram indices obtained were then subjected to four different MANOVAs: two MANOVAs assessing differences between the two groups, and two MANOVAs assessing differences between white and grey matter within each group. The effect size of the analyses was calculated using the partial eta-squared, which represents the ratio between the variance explained by the factor of interest and the sum of the total variance and the variance of the error. The partial eta-squared represents, in this context, the proportion of variance explained by the group factor. The multivariate analyses were performed using both the histograms extracted from the original AV-45 white matter images and those extracted from eroded white matter images, in order to control for spill-out effect. A supplementary multivariate analysis was performed on histogram parameters extracted from AV-45 white matter images masked for hyperintensities.

For both grey and white matter, the difference between groups for each index was tested using canonical univariate analysis.

Classification

Discriminant analysis

In order to assess whether histogram analysis may improve the ability of classical quantitative SUVr assessment to discriminate AD patients from HC participants [8, 22], three different discriminant analyses were performed: an analysis using individual mean SUVr only, a second analysis combining all the histogram indices and a third analysis combining the two previous ones. These analyses were performed on white and grey matter separately and then both taken together. These analyses, performed in Matlab (Statistic Toolbox), were cross-validated using the leave-one-out technique.

For each discriminant analysis, the specificity and sensitivity were calculated. The specificity was defined as the percentage of healthy controls correctly classified (i.e. the percentage of true negatives). The sensitivity was defined as the percentage of AD patients correctly classified (i.e. the percentage of true positives).

Histogram-based cluster analysis

In order to obtain a data-driven classification of the subjects on the basis of their histograms—without feeding the model with a diagnostic label—the white and grey matter histogram indices were subjected to a cluster analysis performed in the Matlab environment. This analysis was based on k-means clustering repeated 20 times, maximizing the cosine distance between cluster centroids. Three models with two, three and four clusters were implemented and the model with the best fit (calculated as the mean of the silhouette values) was kept.

Results

Population

Twenty-four prodromal AD patients and 17 healthy controls, matched in age, gender, and level of education, were recruited. Table 1 reports their demographic and neuropsychological data.

Visual analysis

Three of the 24 AD patients were classified as AV-45 negative and two of the 17 HC subjects were classified as AV-45

Table 1 Demographic and neuropsychological data for the Alzheimer patient (AD) and healthy control (HC) groups

	AD patients	HC subjects	
Age	72.5(±4.9)	69.9(±4.8)	p=0.077
Gender	12 M/12 F	7 M/10 F	χ^2=0.491
Level of education (Years)	11.4(±2.7)	12.8(±3.3)	p=0.193
CDR-scale score	0.6(±0.2)	.0(±.0)	p<.001
MMSE (/30)	24.9(±2.4)	28.4(±0.7)	p<0.001*

M male; *F* female. *CDR* clinical dementia rating

*p<0.05

positive. The visual assessments led to a specificity of 88.2 % and a sensitivity of 87.5 % (see Table 2). Fleiss' kappa was equal to 0.80, indicating substantial agreement between raters.

SUVr comparisons

White and grey matter between groups

In the white matter, there was no significant difference regarding mean SUVr between the two groups (mean for HC=1.92±0.23; mean for AD patients=1.97±0.3, p=.585). Mean SUVr of grey matter was significantly higher for AD patients (1.56±0.3) than for HC participants (1.22±0.1, t=4.36, p<0.001).

White versus grey matter within group

The mean intensity value was significantly higher in white matter than in grey matter in both groups (t=−15.98 for HC participants, t=−13.06 for AD patients, p<0.001 for both groups).

Histogram comparisons

Comparison of white and grey matter histograms between groups

AD grey and white matter histograms seemed, as a whole, to have greater area in the right half of the graph, meaning a higher frequency of high-intensity voxels relative to HC (Fig. 2a-b). Visually, white and grey matter histograms were closer for AD patients than for healthy controls. The Euclidean distance between peaks of the grey and white matter histograms was higher in the HC group (mean=63.74±17.30) than in the AD group (mean=37.19±16.61, t=−4.99, p<0.0001). The same analysis performed using the histograms obtained from the eroded AV-45 white matter images led to comparable results (see Supplementary Table 1).

Comparison of white and grey matter histograms within each group

The shapes of white and grey matter histograms were different for HC and AD groups. This was confirmed by significant differences on multivariate analysis (Lambda=0.4, p<0.05 for AD and Lambda=0.09, p<0.0005 for HC).

As for the multivariate analyses, both white (Lambda=5.2, p<0.001, partial eta-squared=0.51) and grey (Lambda=5.9, p<0.001, partial eta-squared=0.59) matter histograms differed between AD and HC subjects. The MANOVA performed on white matter histogram parameters remained significant when white matter images masked for hyperintensities were used (see supplementary data). Regarding the white matter histograms, only kurtosis, skewness and maximum frequency significantly diverged in the two samples. While kurtosis, skewness and

Table 2 Specificity and sensitivity values for each discriminant analysis and for the visual rating of AV-45 PET scans. The discriminant analyses were performed using the SUVr only (SUVr only), the histogram indices (histogram only), and both histogram indices and SUVr (all). Specificity, sensitivity, and number of false positives (FP) and false negatives (FN) are mentioned for each analysis. False positive refers to healthy controls classified as AD in the discriminant analyses or in the visual rating. False negative refers to AD patients classified as healthy controls in the discriminant analyses or in the visual ratings. The analysis leading to the best trade-off between the two measures is in bold

	Parameters	Specificity	Sensitivity	FP	FN
SUVr	Grey SUVr only	82.4 %	79.2 %	3	5
	White SUVr only	35.3 %	54.2 %	11	7
	Grey and White SUVr only	29.4 %	95.8 %	12	1
Histogram indices	**Grey histogram only**	**88.2 %**	**91.7 %**	**2**	**2**
	White histogram only	58.8 %	87.5 %	7	3
	Grey and White histogram only	76.5 %	83.3 %	4	4
SUVr and histogram indices	Grey All	82.3 %	87.5 %	3	3
	White All	58.8 %	83.3 %	7	4
	Grey and White All	76.5 %	83.3 %	4	4
Visual rating		88.2 %	87.5 %	2	3

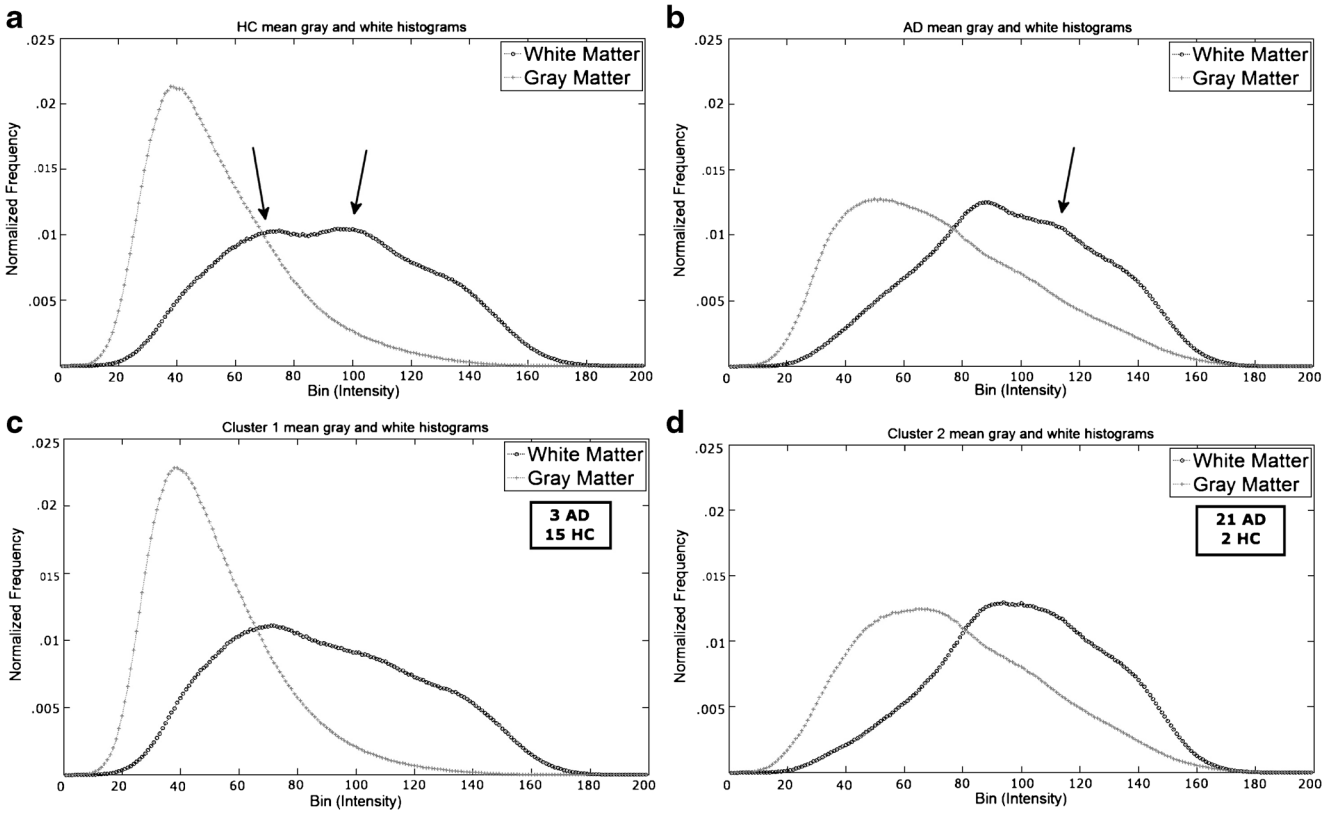

Fig. 2 Mean histogram shapes. *Upper row*: grey and white matter mean histograms for **a** HC and **b** AD groups. *Lower row*: grey and white matter mean histograms for **c** subjects classified in cluster 1 and **d** subjects classified in cluster 2 (cf. the Cluster Analysis section). *Arrows* in (**a**) show shape difference relative to (**c**); *arrow* in (**b**) shows shape difference relative to (**d**), see Cluster Analysis below

maximum frequency were higher in the AD groups, the histogram width was larger for HC subjects (Fig. 2). As for the grey matter histograms, the univariate analyses performed on each index revealed that all the indices were significantly different between the two groups. Median, maximal bins, and ABM were higher for AD groups, while the four other indices were higher for the HC group (Fig. 2). Figure 3 reports the mean indices for grey and white matter in spider-web graphs for the two groups. The same analysis performed using the histograms obtained from the eroded AV-45 white matter images led to comparable results (see Supplementary Table 1).

Probability gradient

Histograms derived from the different thresholds chosen did not show marked changes on visual assessment, confirming the validity of grey and white matter segmentation (see supplementary Figure 1).

Classification

Discriminant analyses

Discriminant analyses on either SUVr values or histogram indices alone, or both SUVr and histogram indices, always showed higher specificity and sensitivity for grey matter only. Discriminant analysis using SUVr values led to better specificity and sensitivity when only grey matter was taken into account (82.4 % and 79.2 %, respectively), compared to white matter only (35.3 % and 54.2 %, respectively) or both grey and white matter (29.4 % and 95.8 % respectively).

Similarly, discriminant analyses on histogram parameters only showed that specificity and sensitivity were higher when only account grey matter was taken into account (88.2 % and 91.7 %, respectively), compared to white matter only (58.8 % and 87.5 %, respectively) or both grey and white matter (76.5 % and 83.3 % respectively).

Discriminant analyses using both histogram parameters and SUVr showed better specificity and sensitivity with grey matter only (82.3 % and 87.5 %, respectively), compared to white matter only (58.8 % and 83.3 %, respectively) or both grey and white matter (76.5 % and 83.3 %, respectively).

Overall, the best trade-off between specificity and sensitivity (the smallest proportion of misclassified patients associated with the smallest proportion of misclassified HC subjects) was reached using grey matter histogram indices *without* the SUVr (Table 2).

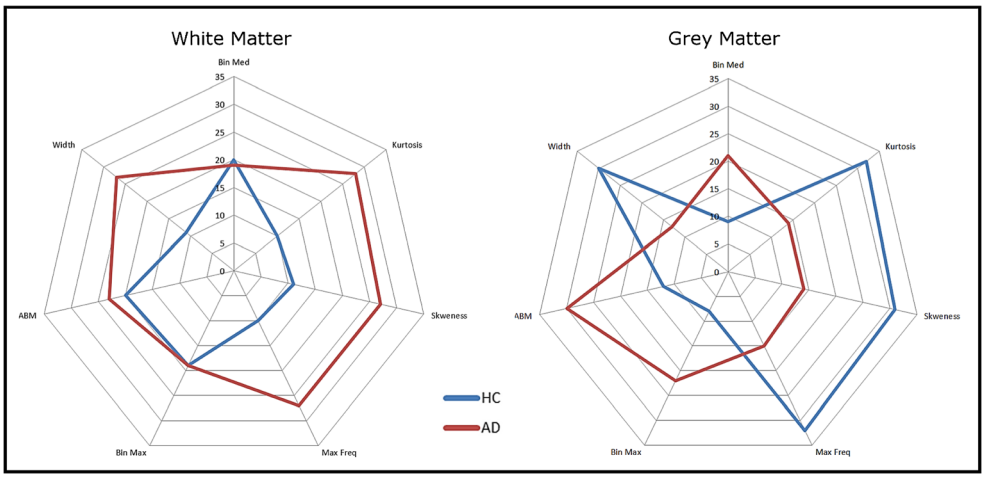

Fig. 3 *Upper panel*. Spider web plots of the seven histogram indices for (HC) and AD patients. Blue line = HC, red line = AD. *Lower panel*. Comparison of the histogram indices in grey matter and in white matter between AD patient and HC subject groups. Mean and (standard deviation) are mentioned for each index. Threshold significance for $p = 0.05$. Significant p values are marked with an *asterisk*

		HC	*AD patients*	*F test*	*p*
Grey Matter					
	Bin Med	8.53 (±2.60)	20.74 (±4.86)	14.24	<.001*
	Kurtosis	31.73 (±3.44)	15.00 (±5.65)	22.30	<.001*
	Skweness	31.53 (±3.60)	15.17 (±5.74)	20.09	<.001*
	Max Freq	31.27 (±3.94)	15.43 (±5.72)	17.73	<.001*
	Bin Max	7.60 (±2.03)	21.57 (±4.56)	24.18	<.001*
	ABM	11.67 (±3.32)	28.70(±5.60)	27.50	<.001*
	Width	30.20 (±4.01)	16.04 (±6.20)	12.92	<.001*
White Matter					
	Bin Med	18.53 (±4.49)	19.40 (±4.66)	.34	.441
	Kurtosis	12.20 (±5.01)	28.09 (±4.91)	26.92	<.0001*
	Skweness	12.67(±5.41)	27.61(±5.10)	21.39	<.0001*
	Max Freq	12.93 (±5.80)	27.26 (±5.09)	17.01	<.0001*
	Bin Max	19.27(±5.06)	20.51 (±5.35)	.41	.530
	ABM	21.93(±6.66)	23.61(±5.46)	.17	.547
	Width	14.80 (±7.06)	25.96 (±4.93)	9.94	<.005*

It is noteworthy that, when the analysis relied on grey and white matter together, adding the mean SUVr to histogram indices did not improve the classification performance.

The histograms of misclassified subjects were plotted with AD and HC mean histograms (Fig. 4). For grey-matter-based classification (Fig. 4a), the two misclassified healthy controls had part of the histogram beyond the 75th percentile of the AD grey matter mean histogram. As for the two misclassified AD, their histograms had both higher peaks and narrower curves than the AD mean histogram.

Regarding histograms of the white matter only, we selected four misclassified subjects (two AD and two HC) for easier reading of the figure (Fig. 4b), as profiles were very heterogeneous (see supplementary Figure 2). Two of them, one AD and one HC, showed right-shifted histograms with peaks

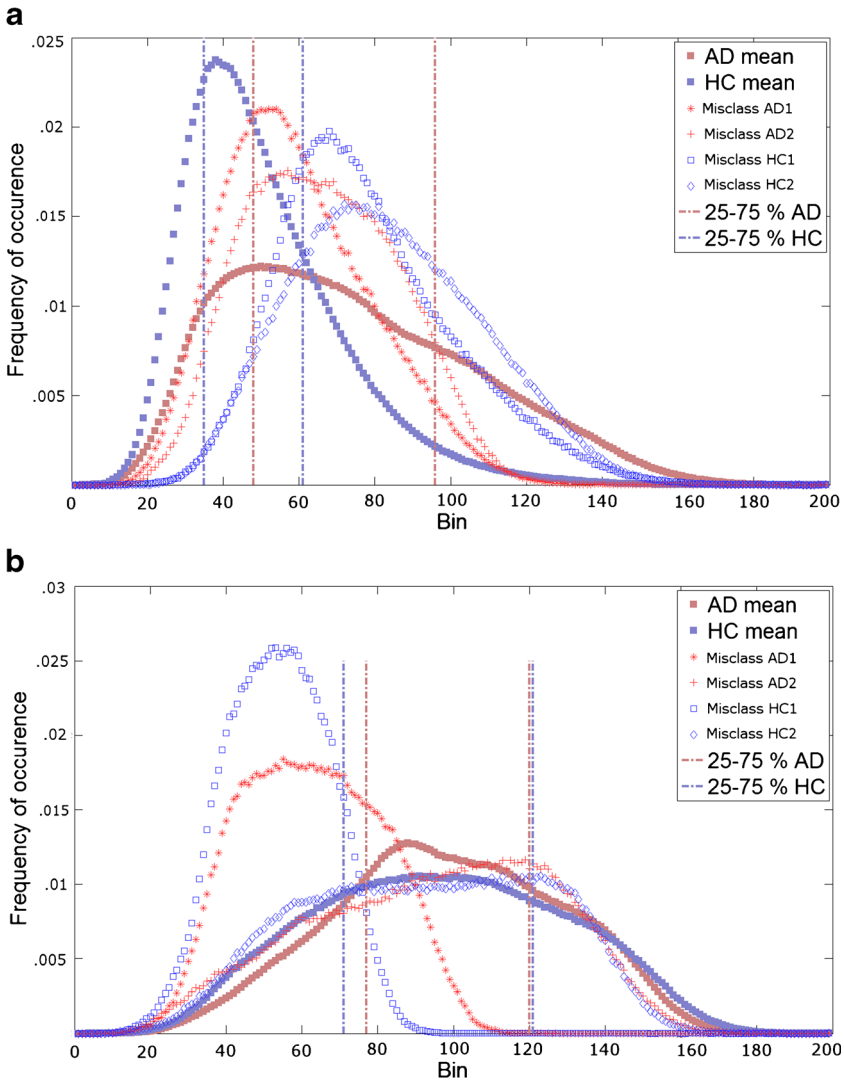

Fig. 4 Histogram shape for misclassified subjects. **a** Grey matter mean histograms of the two AD patients classified as HC (*red stars* and *red crosses*) and the two HC classified as AD (*empty blue squares* and *diamonds*) in the discriminant analysis performed on grey matter histogram parameters plotted against the mean grey matter histogram of the correctly classified AD (*filled red square*) and HC (*blue filled square*). **b** White matter mean histograms of two (out of three) AD patients classified as HC (*red stars* and *red crosses*) and the two (out of seven) HC classified as AD (*empty blue squares* and *diamonds*) in the discriminant analysis performed on white matter histogram parameters, plotted against the mean white matter histogram of the correctly classified AD (*filled red squares*) and HC (*blue filled squares*). One out of three misclassified AD and five out of seven misclassified HC are not shown for ease of presentation; see supplementary Figure 2. Vertical dashed-dotted lines in panels **a** and **b** mark 25th and 75th percentiles of histograms

below the 25th percentiles of their respective groups' mean histograms. The other two showed histogram shapes similar to those of their respective groups.

Cluster analysis

The cluster analysis performed on the grey and white matter histogram indices revealed that the best model (i.e. the solution with the lowest mean silhouette value) was based on two clusters. Cluster 1 comprised three AD patients and 15 HC, while cluster two comprised 21 AD patients and two HC. Cluster 1 and cluster 2 mean histogram shapes were similar to those of HC and AD, respectively (Fig. 2). However, some shape differences could be observed between Cluster 1 and HC mean histograms, and between Cluster 2 and AD mean histograms, in particular for the white matter. It is noteworthy that the subjects who were misclassified in the discriminant analyses did not belong to the same cluster.

Discussion

The aim of this study was to compare patterns of AV-45 uptake in white matter of Alzheimer's disease patients and healthy controls, and to compare AV-45 uptake in white and grey matter within these two groups.

As expected, we showed that AV-45 uptake in grey matter was higher in AD patients than in HC using SUVr analysis. However, white matter uptake was higher than grey matter uptake in both groups, using the same method. Despite the lack of difference found between the two groups in white matter using SUVr, our innovative AV-45 uptake assessment using histograms showed differences between the two groups within this tissue. Such difference in AD and HC white matter histograms was also present when the comparison involved the histograms derived from the eroded AV-45 white matter images. This suggests that the difference cannot be attributed to a spill out of the AV-45 signal from the grey to the white matter. However, inclusion of white matter in the discriminant

analysis did not improve the classification performance, but the histogram indices outperformed SUVr in such classification. To our knowledge, no other study has investigated differential AV-45 uptake in white and grey matter of AD patients and healthy controls.

Regarding grey matter, the mean SUVr was higher for AD patients than for healthy controls. These results confirm that amyloid deposition in the AD patients' grey matter, as measured by AV-45 SUVr, is significantly higher than in healthy controls [4, 6]. Recent work using MRI-based segmentation methods have shown similar results in prodromal AD patients [7]. The histogram analysis also showed a significant difference between the two groups on every index used.

In white matter, mean SUVr was higher than in grey matter for both groups. This result confirms the highly lipophilic nature of AV-45 [1, 8, 9]. No difference was found on SUVr analyses between groups of prodromal AD patients and healthy controls, a finding in line with previous reports using different amyloid markers like PiB [13, 14] and florbetaben [12, 13]. Interestingly, histogram analyses did reveal significant differences in this tissue, as patients with AD showed greater width, kurtosis, skewness and maximum frequency than healthy controls. This difference suggests that not all uptake in white matter is non-specific. This kind of result has never been shown using AV-45 PET imaging. However, using other imaging modalities, such as MRI, white matter modifications (e.g. axonal injury and white matter tract degradation) in AD patients have recently been discovered [23–25]. In their study, Zhang and colleagues showed a reduction of fractional anisotropy (FA) using DTI sequences in a group of AD patients, while Canu and colleagues (2011) found increased mean diffusivity (MD) in AD patients in several cortical tracts. Such results are consistent with white matter tract degradation. These modifications may be related to the differences observed in our study between the AD and the HC white matter, and further work is needed to determine the cause of the differences that we report. Apart from white matter microstructural changes revealed by DTI imaging, the difference we observed between AD and HC white matter histograms may be related to white matter hyperintensities (WMHs). WMH volumes have been shown to be associated with cognitive performance in AD patients more than in MCI and HC [26]. Moreover, WMHs are more hypoperfused in AD patients than in HC [27]. However, to our knowledge, there are no studies focusing on the relationship between AV-45 uptake in the white matter and WMHs, although a study performed using PiB showed that amyloid burden is correlated with the index of microstructural damage in WMHs [28]. In the present study, WMHs did not seem to explain the observed difference (see supplementary data). Future investigations, including FLAIR imaging, will be necessary to shed light on this topic. Independently of the pathophysiological causes of differences in histograms, analysis of the intensity histogram may be able to reveal pathological changes in the AD white matter that are overshadowed by non-specific binding when only mean SUVr is taken into account. Incidentally, it is worth noting that grey and white matter histograms look alike in the AD sample, and that the Euclidean distance between grey matter and white matter peaks is diminished compared to healthy controls. Moreover, in Fig. 3, AD grey matter plots resemble HC white matter plots. This may suggest similar properties of grey matter tissue in AD and white matter tissue in HC. Further investigations using multimodal PET amyloid and MRI imaging in the same sample would be required to understand this phenomenon. Observing differential AV-45 white matter uptake in a pathological population compared to healthy subjects speaks in favour of the possibility of using such a marker to study diseases related to white matter disorders. Indeed, some studies have already used PiB to study white matter status in different pathologies or neurological conditions. In particular, PiB has been used to investigate white matter modifications after traumatic brain injury [29] and in leukoaraiosis [28, 30]. The latter studies found that PiB uptake in the white matter was correlated to WMH volume in cerebral amyloid angiopathy patients but not in AD patients [30], and that PiB positivity in the white matter was associated with reduction of the fractional anisotropy [28]. To our knowledge, AV-45 has not yet been used for investigating white matter pathologies.

Despite the significant difference in white matter AV-45 uptake between AD and HC as shown by histogram analysis in our study, discriminant analyses suggest that white matter is not useful to classify AD and HC subjects. While discriminant analyses based only on grey matter histogram indices led to highest specificity and sensitivity, white-matter–based classification showed a high sensitivity, but dramatically poor specificity. When indices of both grey and white matter histograms were used, the performance of the discriminant model was worse, suggesting that white matter brings noise in the classification. A few studies on amyloid markers have also reported good classification performance using different methods. A recent study using the amyloid marker flutemetamol showed a specificity of 92 % and a sensitivity of 85.2 % in discriminating patients with mild cognitive impairment (MCI) from HC, using a learning machine method [25]. Discriminant analyses in AD have also been widely used in other modalities such as MRI [31], or combinations of modalities [32, 33]. In their classification study based on combined features of structural MRI sequences, Wolz et al. reported a specificity of 85 % and sensitivity of 93 % for discrimination between AD and HC, but only a specificity of 82 % and sensitivity of 86 % between patients with MCI and HC [34]. Of note, white matter histograms in our analysis showed great variability (Fig. 4), which could be the reason why white matter indices do not improve the classification.

Several white matter modifications related to ageing have been described in the MRI literature [35–37]. Moreover, it has been shown that vascular amyloid deposit increases with age, which may lead to significant AV-45 uptake. Taken together, these age-related modifications may partly explain the observed variability in white matter histogram profiles. These hypotheses would require further investigation, targeting these issues directly.

The evidence from the discriminant analysis should be read together with the results of the cluster analysis, in which the classification was performed without the a priori label of the diagnosis. The best solution was a model with two clusters, confirming that two general white and grey histogram intensity profiles were present in the two samples. These two clusters roughly correspond to the two diagnostic samples of the study. We propose that the two clusters would correspond to "AV-45 binder" and "AV-45 non-binder" as the leftward peak of the mean histogram for cluster one grey matter clearly represents low fixation (non-binder, Fig. 2a), while the histogram shape for cluster 2 suggests high uptake values (binder, Fig. 2b). Moreover, total non-specific binding in the white matter should lead to a comparable (high) AV-45 fixation in the two groups. The presence of significant differences in white matter histograms suggests that some form of specific binding exists in the white matter.

As a final note, the finding that four AD patients were amyloid negative and two healthy controls were amyloid positive on visual assessment is in line with the findings in the literature [9, 6]. More interesting is the convergence between visual rating and cluster analysis, two methods without any a priori. Comparing the members of the two clusters and the visual assessment results, we found that the two HC members of cluster number 2, which contained mainly AD patients, were the same HC rated as amyloid-positive on visual analysis. In the same way, the three AD patients classified in cluster number 1, which contained mainly HC, were rated as amyloid-negative on visual assessment. Compared to these two methods without a priori, the analysis with a priori (i.e. discriminant analysis) showed slightly better classification performance. This suggests that a discriminant model based on clinical information should be favoured over an unsupervised model.

Conclusion

In this study, we first demonstrated differential AV-45 binding in white matter between patients with Alzheimer's disease at an early stage and healthy controls. White matter binding is thus not exclusively non-specific, as is sometimes proposed. This information is not detectable using a mean SUVr approach, but becomes clear when histogram index analyses are performed. Our results suggest that white matter AV-45 uptake, although not useful in discriminating between AD patients and HC, may carry information on white matter integrity and contribute to the study of white matter in these populations. We also show that the use of grey matter histogram indices reaches the best sensitivity and specificity for AD and HC discrimination. Such results demonstrate that the histogram approach could be useful in clinical practice.

Acknowledgments This study was supported by a grant from the University Hospital of Toulouse, local grant 2007, and a grant from the Agence Nationale de la Recherche. The authors thank the promoter of this study and Toulouse University Hospital.

Conflict of interest The authors declare that they have no conflict of interest.

References

1. Choi SR et al. Preclinical properties of 18F-AV-45: a PET agent for Abeta plaques in the brain. J Nucl Med. 2009;50(11):1887–94.
2. Carpenter Jr AP et al. The use of the exploratory IND in the evaluation and development of 18F-PET radiopharmaceuticals for amyloid imaging in the brain: a review of one company's experience. Q J Nucl Med Mol Imaging. 2009;53(4):387–93.
3. Clark CM et al. Cerebral PET with florbetapir compared with neuropathology at autopsy for detection of neuritic amyloid-beta plaques: a prospective cohort study. Lancet Neurol. 2012;11(8):669–78.
4. Clark CM et al. Use of florbetapir-PET for imaging beta-amyloid pathology. JAMA. 2011;305(3):275–83.
5. Lin KJ et al. Whole-body biodistribution and brain PET imaging with [18F]AV-45, a novel amyloid imaging agent–a pilot study. Nucl Med Biol. 2010;37(4):497–508.
6. Wong DF et al. In vivo imaging of amyloid deposition in Alzheimer disease using the radioligand 18F-AV-45 (florbetapir [corrected] F 18). J Nucl Med. 2010;51(6):913–20.
7. Saint-Aubert L et al. Cortical florbetapir-PET amyloid load in prodromal Alzheimer's disease patients. Eur J Nucl Med Mol Imaging. 2013;3(1):43.
8. Camus V et al. Using PET with 18F-AV-45 (florbetapir) to quantify brain amyloid load in a clinical environment. Eur J Nucl Med Mol Imaging. 2012;39(4):621–31.
9. Fleisher AS et al. Using positron emission tomography and florbetapir F18 to image cortical amyloid in patients with mild cognitive impairment or dementia due to Alzheimer disease. Arch Neurol. 2011;68(11):1404–11.
10. La Joie R et al. Region-specific hierarchy between atrophy, hypometabolism, and beta-amyloid (Abeta) load in Alzheimer's disease dementia. J Neurosci. 2012;32(46):16265–73.
11. Rodrigue KM et al. beta-Amyloid burden in healthy aging: regional distribution and cognitive consequences. Neurology. 2012;78(6):387–95.
12. Villemagne VL et al. Amyloid imaging with (18)F-florbetaben in Alzheimer disease and other dementias. J Nucl Med. 2011;52(8):1210–7.
13. Villemagne VL et al. Comparison of 11C-PiB and 18F-florbetaben for Abeta imaging in ageing and Alzheimer's disease. Eur J Nucl Med Mol Imaging. 2012;39(6):983–9.
14. Fodero-Tavoletti MT et al. Characterization of PiB binding to white matter in Alzheimer disease and other dementias. J Nucl Med. 2009;50(2):198–204.

15. Dubois B et al. Research criteria for the diagnosis of Alzheimer's disease: revising the NINCDS-ADRDA criteria. Lancet Neurol. 2007;6(8):734–46.
16. Wallon D et al. The French series of autosomal dominant early onset Alzheimer's disease cases: mutation spectrum and cerebrospinal fluid biomarkers. J Alzheimers Dis. 2012;30(4):847–56.
17. Fleiss JL, Nee JCM, Landis JR. Large sample variance of kappa in the case of different sets of raters. Psychol Bull. 1979;86(5): 974–7.
18. Kyriazi S et al. Metastatic ovarian and primary peritoneal cancer: assessing chemotherapy response with diffusion-weighted MR imaging–value of histogram analysis of apparent diffusion coefficients. Radiology. 2011;261(1):182–92.
19. Pope WB et al. Recurrent glioblastoma multiforme: ADC histogram analysis predicts response to bevacizumab treatment. Radiology. 2009;252(1):182–9.
20. Pope WB et al. Apparent diffusion coefficient histogram analysis stratifies progression-free survival in newly diagnosed bevacizumab-treated glioblastoma. AJNR Am J Neuroradiol. 2011;32(5):882–9.
21. Conover WJ, Iman RL. Rank transformations as a bridge between parametric and nonparametric statistics—rejoinder. Am Stat. 1981;35(3):132–3.
22. Barthel H et al. Cerebral amyloid-beta PET with florbetaben (18F) in patients with Alzheimer's disease and healthy controls: a multicentre phase 2 diagnostic study. Lancet Neurol. 2011;10(5):424–35.
23. Canu E et al. Mapping the structural brain changes in Alzheimer's disease: the independent contribution of two imaging modalities. J Alzheimers Dis. 2011;26 Suppl 3:263–74.
24. Firbank MJ et al. Diffusion tensor imaging in Alzheimer's disease and dementia with Lewy bodies. Psychiatry Res. 2011;194(2): 176–83.
25. Vandenberghe R et al. Binary classification of ^{18}F-flutemetamol PET using machine learning: comparison with visual reads and structural MRI. Neuroimage. 2013;64:517–25.
26. Kim JH et al. Regional white matter hyperintensities in normal aging, single domain amnestic mild cognitive impairment, and mild Alzheimer's disease. J Clin Neurosci. 2011;18(8):1101–6.
27. Makedonov I, Black SE, MacIntosh BJ. Cerebral small vessel disease in aging and Alzheimer's disease: a comparative study using MRI and SPECT. Eur J Neurol. 2013;20(2):243–50.
28. Chao LL et al. Associations between white matter hyperintensities and beta amyloid on integrity of projection, association, and limbic fiber tracts measured with diffusion tensor MRI. PLoS One. 2013;8(6):e65175.
29. Hong YT, et al. Amyloid imaging with carbon 11-labeled Pittsburgh compound B for traumatic brain injury. JAMA Neurol. 2014;71(1): 23–31.
30. Gurol ME, et al. Cerebral amyloid angiopathy burden associated with leukoaraiosis: A positron emission tomography/magnetic resonance imaging study. Ann Neurol. 2013;73(4):529–536.
31. Casanova R, Hsu F-C, Espeland MA, Alzheimer's Disease Neuroimaging Initiative. Classification of structural MRI images in Alzheimer's disease from the perspective of ill-posed problems. PLoS One. 2012;7(10):e44877.
32. Jagust W et al. What does fluorodeoxyglucose PET imaging add to a clinical diagnosis of dementia? Neurology. 2007;69(9):871–7.
33. Westman E, Muehlboeck JS, Simmons A. Combining MRI and CSF measures for classification of Alzheimer's disease and prediction of mild cognitive impairment conversion. Neuroimage. 2012;62(1):229–38.
34. Wolz R et al. Multi-method analysis of MRI images in early diagnostics of Alzheimer's disease. PLoS One. 2011;6(10):e25446.
35. Jeon T et al. Regional changes of cortical mean diffusivities with aging after correction of partial volume effects. Neuroimage. 2012;62(3): 1705–16.
36. Stadlbauer A et al. Magnetic resonance fiber density mapping of age-related white matter changes. Eur J Radiol. 2012;81(12):4005–12.
37. Watanabe H et al. Progression and prognosis in multiple system atrophy: an analysis of 230 Japanese patients. Brain. 2002;125(Pt 5):1070–83.